

The connectivity degree controls the difficulty of RBN reservoir design

Emmanuel Calvet^{1,*}, Bertrand Reulet² and Jean Rouat¹

¹NECOTIS, Faculté de Génie, GEGI, Université de Sherbrooke, Québec, Canada

²Institut Quantique, Faculté des Sciences, Département de Physique, Université de Sherbrooke, Québec, Canada

Correspondence*:

2500, boulevard de l'Université Sherbrooke, J1K 2R1, Québec, Canada

emmanuel.calvet@usherbrooke.ca

2 ABSTRACT

3 Reservoir Computing (RC) is a paradigm in artificial intelligence where a recurrent neural
4 network (RNN) is used to process temporal data, leveraging the inherent dynamical properties
5 of the reservoir to perform complex computations. In the realm of RC, the excitatory-inhibitory
6 balance b has been shown to be pivotal for driving the dynamics and performance of Echo State
7 Networks (ESN) and, more recently, Random Boolean Network (RBN). However, the relationship
8 between b and other parameters of the network is still poorly understood. This article explores
9 how the interplay of the balance b , the connectivity degree K (i.e., the number of synapses per
10 neuron) and the size of the network (i.e., the number of neurons N) influences the dynamics and
11 performance (memory and prediction) of an RBN reservoir. Our findings reveal that K and b are
12 strongly tied in optimal reservoirs. Reservoirs with high K have two optimal balances, one for
13 globally inhibitory networks ($b < 0$), and the other one for excitatory networks ($b > 0$). Both show
14 asymmetric performances about a zero balance. In contrast, for moderate K , the optimal value
15 being $K = 4$, best reservoirs are obtained when excitation and inhibition almost, but not exactly,
16 balance each other. For almost all K , the influence of the size is such that increasing N leads to
17 better performance, even with very large values of N . Our investigation provides clear directions
18 to generate optimal reservoirs or reservoirs with constraints on size or connectivity.

19 **Keywords:** Reservoir Computing, RBN, Criticality, Topology, Memory, Prediction

1 INTRODUCTION

20 Reservoir computing (RC) is a promising approach that could drastically reduce the cost of learning as the
21 input gets projected into a higher dimensional space, *the reservoir*, read out by a single output layer. As
22 such, when the reservoir is adequately designed, a simple linear fitting can be used to train the weights of
23 the readout layer (Maass u. a., 2002), alleviating the computational burden of other traditional machine
24 learning methods. The Echo State Network (ESN) developed by (Jaeger, 2005) comprises reservoirs with
25 continuous activation functions, while Liquid State Machine (LSM) (Maass u. a., 2002) typically includes
26 discontinuous activation functions, among which we find the Random Boolean Network (RBN) (Glass und
27 Hill, 1998).

28 The connectivity degree has been extensively studied in RBN reservoirs, and in contrast to ESN, it
29 displays desirable dynamics for very sparse matrices (Luque und Solé, 2000; Bertschinger und Natschläger,
30 2004; Büsing u. a., 2010; Snyder u. a., 2012; Echlin u. a., 2018), while ESN was shown to be less sensitive
31 to this parameter (Hajnal und Lörincz, 2006; Büsing u. a., 2010; Krauss u. a., 2019a; Metzner und Krauss,
32 2022). On the other hand, it is well known that increasing the number of neurons improves performance
33 (Bertschinger und Natschläger, 2004; Snyder u. a., 2012; Cherupally, 2018; Cramer u. a., 2020; Steiner
34 u. a., 2023). However, most literature on RBN compared reservoirs with rather small sizes around 1000
35 neurons (Bertschinger und Natschläger, 2004; Natschläger u. a., 2005; Büsing u. a., 2010; Snyder u. a.,
36 2013; Burkow und Tufte, 2016), while studies on the ESN compared reservoirs from 500, up to 20000
37 neurons (Triefenbach u. a., 2010).

38 In this article, we want to study the effect of these topology parameters (N and K), with another control
39 parameter, which is the excitatory-inhibitory balance b , controlling the proportion of positive and negative
40 synaptic weights (Krauss u. a., 2019a; Metzner und Krauss, 2022; Calvet u. a., 2023). The balance is
41 equal to $b = (S_+ - S_-)/S$, with $S = KN$ the total number of synapses and S_{\pm} the number of positive
42 and negative synapses. For a positive balance, the network has a majority of excitatory synapses and
43 reverse, and when it is zero, the network has a perfect balance between the two, $S_+ = S_-$. Previous
44 work on the ESN (Krauss u. a., 2019b,a; Metzner und Krauss, 2022) has studied the influence of density
45 $d = K/N$ and balance on the dynamics of reservoirs, showing that b was a key parameter controlling
46 phase transitions. In particular, the edge of chaos, a dynamical phase transition between order and chaos,
47 is believed to be fundamental in reservoir design, for a reservoir to acquire computational capabilities
48 (for a comprehensive introduction, see (Legenstein und Maass, 2006; Nowshin u. a., 2020)). Nevertheless,
49 Metzner *et al.* suggested a more complex picture than previously thought, exposing two critical points,
50 each for a positive and negative balance, while for higher densities, an asymmetry could arise in the
51 reservoir responses to inputs, and as a result, only the edge of chaos occurring for positive b was optimal
52 for information propagation inside the reservoir (Metzner und Krauss, 2022).

53 In line with Krauss and Metzner, recent work on RBN reservoirs demonstrated that the excitatory-
54 inhibitory balance b was also key in driving dynamics and performance (Calvet u. a., 2023). In particular, it
55 was shown that the weight statistics, typically used in RBN literature (Bertschinger und Natschläger, 2004;
56 Natschläger u. a., 2005; Büsing u. a., 2010) are related to the balance. More striking, the RBN reservoirs
57 also displayed an asymmetry around $b = 0$. The two signs of the balance produced distinct relations to
58 performance in tasks and a reduced reservoir-to-reservoir variability for a majority of inhibition. However,
59 this occurred for a network with extremely low density as $d = K/N = 16/10000 = 0.0016$, in contrast
60 with studies on ESN.

61 As far as the authors are aware, the influence of the excitatory-inhibitory balance for different connectivity
62 has yet to be studied, except for the single value of $K = 16$ previously mentioned (Calvet u. a., 2023). This
63 article aims to explore the combined effect of connectivity (K, N) and the balance on the dynamics and
64 performance of the RBN. The article is organized as follows: in the first section (Sec. 3.1) the effect of K
65 and b is studied, both on the dynamics of free-evolving reservoirs (Sec. 3.1.1), and their performance in a
66 memory and prediction task (Sec. 3.1.2), showing that the asymmetry in fact vanishes for very small K .
67 In the second section (Sec. 3.2) we perform a similar analysis (dynamics in Sec. 3.1.1, and performance
68 in Sec. 3.2.2), but this time, we vary both K and N conjointly, and explore the relationship with b . This
69 reveals a complex interplay between parameters and suggests that K is, in fact, governing it. Finally, in
70 Sec. 4, we discuss our results and their implication for RBN reservoir design, revealing that in contrast

71 with *ESN*, the careful selection of K leads to a significant simplification of the fine-tuning of the other
 72 topology parameters in the tested tasks.

2 METHODOLOGY

73 2.1 The model

74 Our model is an ensemble of three parts (Fig. 1), the input node $u(t)$, which is projecting to half of the
 75 neurons of the recurrently connected reservoir \vec{x} , among which the other half is projecting to the output
 76 node $y(t)$, this way, the output node never directly sees the input, and information must propagate inside
 77 the reservoir for the readout to accomplish the task at hand:

$$u_i(t) = w_i^{in} u(t) \quad (1)$$

$$y(t) = f(W^{out} \vec{x} + c) \quad (2)$$

78 With $u_i(t)$ the input of the neuron i , the input weights w_i^{in} form a vector, projecting to half of the reservoir,
 79 while the other half of the weights are zeros, and reserve for the output weight matrix W^{out} . This way, a
 80 neuron in the reservoir is never connected to both the input and output. The activation function f of the
 81 output node is the sigmoid, with a bias c . Each component $x_i(t)$ of $\vec{x}(t)$ corresponds to the state of the
 82 neuron i inside the reservoir. It is given by:

$$x_i(t) = \theta \left(u_i(t) + \sum_{j=1}^N w_{ij} x_j(t-1) \right) \quad (3)$$

83 Where each neuron is connected to K other neurons, and w_{ij} is the synaptic weight connecting neuron j to
 84 neuron i , drawn in a normal distribution $\mathcal{N}(\mu, \sigma)$, with parameters μ (mean) and σ (standard deviation).
 85 The activation function θ is a Heaviside, thus x_i is binary. $t \in \mathbb{N}$ and corresponds to a time step. Remark
 86 that if the input is zero, the state of a given neuron only depends on the states of its neighbours at the
 87 previous time step. Such neurons are thus said to be "memoryless", and for such a system, to sustain
 88 memory, information needs to cascade via the propagation of spikes inside the reservoir. The attractive
 89 feature of the reservoir framework is that only the output weight and bias are trainable parameters, as all
 90 other parameters are usually kept fixed, including the reservoir weights.

91 We use a mean square error (MSE) loss function for the training process. For training the readout weights,
 92 we opted for the ADAM optimizer (Kingma und Ba, 2015), providing superior results in our testings,
 93 superseding the commonly utilized Ridge regression (Burkow und Tufte, 2016) in most literature. The
 94 execution is facilitated through the PyTorch library, with parameters set at $\alpha = 0.001$ and 4000 epochs
 95 (Supplementary Materials 6 for additional information).

96 2.2 The control parameters

97 The three control parameters used in this study are σ^* , K , and N . Among these, σ^* represents the
 98 coefficient of variation of the weight distribution within the reservoir, defined as $\sigma^* = \sigma/\mu$. This parameter
 99 is linked to b , the excitatory/inhibitory balance, as $b = \text{Erf}[1/(\sqrt{2}\sigma^*)]$ (Calvet u. a., 2023). The balance is

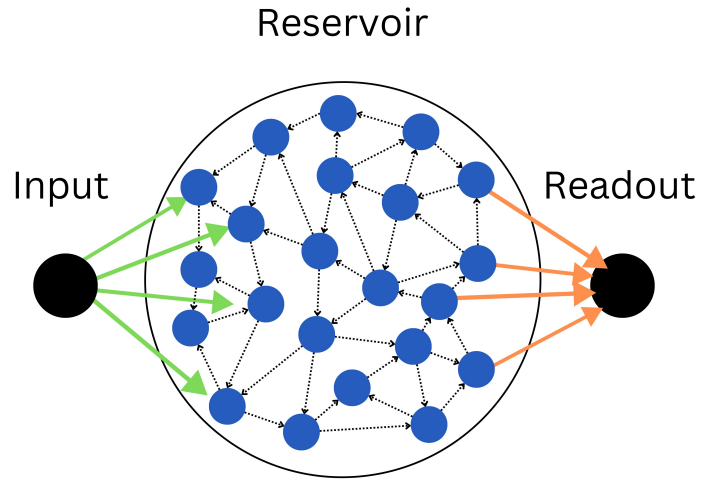


Figure 1. The model consists of an input node (left), connected by input weights (green arrows), to the reservoir (center), itself connecting via output weights (orange arrows) to the output node (right). As illustrated by the dotted black arrows, the reservoir is recurrently connected, forming a random graph. The illustrated graph has $K = 2$ and $N = 22$. Note that in practice, half of the neurons (blue circles) connect to the input, and the other half to the readout.

100 also equal to $b = (S_+ - S_-)/S$, with S the total number of synapses, and S_{\pm} the number of positive and
 101 negative synapses, respectively. We display in Fig. 2 the relationship between the two, noting that when σ^*
 102 is positive, we have a majority of excitatory synapses $b > 0$, and when σ^* is negative, we have a majority
 103 of inhibitory synapses $b < 0$. In all experiments, we play with values of σ^* that allow our reservoirs to span
 104 the full range of b , corresponding to $\sigma^* \in [10^{-2}, 10^3]$.

105 Since recent work showed that the dynamics and performance of reservoirs were asymmetric about $b = 0$
 106 (Metzner und Krauss, 2022; Calvet u. a., 2023), we study the influence of two other control parameters
 107 with respect to the sign of b . These parameters are captured by the density $d = K/N$, following the work
 108 of (Hajnal und Lörincz, 2006; Krauss u. a., 2019a; Metzner und Krauss, 2022) on ESN. However, we show
 109 in supplementary material 6.1 that the density d is not a control parameter for the RBN, since, at a fixed
 110 density, reservoirs can possess very different dynamics as K and N are concurrently varied. As such, we
 111 consider them as independent control parameters in this article. Following work in RBN (Büsing u. a.,
 112 2010; Calvet u. a., 2023), the connectivity degree is chosen between 1 and 16. In addition, to compare
 113 the more recent results ($N = 10000$) (Calvet u. a., 2023) with older literature ($N \leq 1000$) (Bertschinger
 114 und Natschläger, 2004; Natschläger u. a., 2005; Büsing u. a., 2010; Snyder u. a., 2013; Burkow und Tufte,
 115 2016), we study three values of $N = \{100, 1000, 10000\}$.

116 2.3 The experiments

117 We perform two types of tasks: the first to probe the intrinsic dynamics of reservoirs, while they are freely
 118 evolving, and the second to test the ability to process inputs while performing memory and prediction tasks.

119 2.3.1 Free-running

120 Each reservoir is freely running without input for a duration of $D = 2000$ time steps, with a random
 121 initial state with 20% of neurons to one. During a run, the activity signal $A(t)$ (the average of states x_i at a
 122 given time step t) is recorded. Afterward, we compute the BiEntropy (H_b) (Croll, 2014) of the binarized

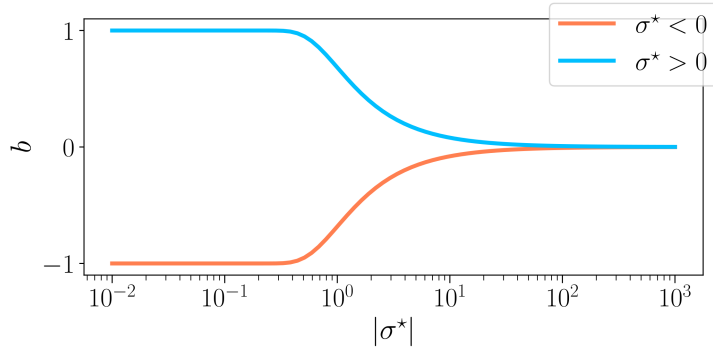


Figure 2. The excitation-inhibition balance b as a function of the synaptic weight parameter σ^* . For $\sigma^* < 0$ (—) and $\sigma^* > 0$ (—). σ^* is the coefficient of variation (σ/μ) of the weight distribution, which is why b is of the sign of σ^* . For low values of $|\sigma^*|$, only μ controls the synaptic balance, meaning that for a positive mean, the weights are all excitatory, and reverse. On the other hand, when $|\sigma^*| \rightarrow \infty$, the mean becomes irrelevant, and b is at a perfect balance between excitation and inhibition.

123 activity signals, which quantify the degree of order and disorder of a bit string, $H_b = 0$ for completely
 124 periodic, and $H_b = 1$ for totally irregular. For each triplet (N, K, σ^*) , we randomly generate 100 reservoirs,
 125 and we then compute the average and variance over reservoirs having the same control parameters.

126 Next, we classify the steady-state activity $A(t)$, for $t > 1000$ time steps, into four distinct attractor
 127 categories. For each triplet (N, K, σ^*) , we then compute the histograms over the 100 reservoirs. The
 128 attractors are defined according to (Calvet u. a., 2023) :

- 129 • **Extinguished:** The activity has died out, and the steady activity is zero at all time steps.
- 130 • **Fixed attractor:** The steady activity is non-zero, but its derivative is zero at all time steps.
- 131 • **Cyclic:** The steady activity repeats, with a period larger than one time-step.
- 132 • **Irregular:** If none of the above categories apply, the signal is irregular. Note that our model is
 133 deterministic and discrete, as such, all attractors are in theory, cyclic; however, since the duration
 134 $D = 2000$ is extremely small compared to the maximal period of 2^N , in practice, we find a statistically
 135 significant proportion of attractors in that category.

136 2.3.2 Performance in tasks

137 To test the computational capabilities of our reservoirs, we perform two distinct tasks. The first one
 138 consists of memorizing white-noise input received $|\delta|$ time steps in the past. We test our reservoirs with
 139 various difficulties for $\delta = \{-18, -14, -10, -6, -2\}$. The higher in absolute value, the more difficult the
 140 task, since it demands the reservoir of memoryless neurons to integrate and reverberate input information
 141 through spikes cascade for longer time scales (Metzner und Krauss, 2022; Calvet u. a., 2023). The second
 142 task consists of predicting Mackey-Glass time series, $\delta = 10$ time steps in the future. Mackey-Glass is
 143 a common benchmark in reservoir computing (Hajnal und Lörincz, 2006; Bianchi u. a., 2016; Zhu u. a.,
 144 2021). We use τ , the time constant parameter of Mackey-Glass, which controls the signal dynamics,
 145 ranging from $\tau = 5$ (periodic), $\tau = 15$, to $\tau = 28$ (chaotic). To evaluate the performance of our reservoir,
 146 we compute the correlation coefficient $Corr(y, T)$ between the target T , and the output y (implementation
 147 details are identical to this study (Calvet u. a., 2023)).

3 RESULTS

148 3.1 The connectivity degree controls the optimal balance

149 In this section, we fix the size of the reservoir to its largest value $N = 10000$. We study the effect of
 150 K and b on the dynamics of free-running reservoirs (Sec. 3.1.1). Then, we study the performance in two
 151 demanding tasks (Sec. 3.1.2). We show that the asymmetry about $b = 0$ is strongly K dependent and
 152 vanishes for low K , while the optimal balance b_{opt} is entirely controlled by K .

153 Additionally, we exhibit the shift of control parameters from the more natural weight distribution statistics
 154 (σ^*) (Calvet u. a., 2023) to the excitatory-inhibitory balance (b). To do so, we begin by exhibiting the
 155 dynamics over σ^* , to then display the attractor statistics over the excitatory balance b , revealing insights
 156 into the reservoir design.

157 3.1.1 Impact of the connectivity degree and balance on dynamics

158 In Fig. 3, we display the average over reservoirs of the BiEntropy of the steady activities for reservoirs as
 159 a function of $|\sigma^*$ (lower x-axis), both with a negative (left) or positive (right) balance b (the upper x-axis
 160 displays the corresponding b values). In Fig. 3.A and B, blue regions represent an ordered phase with
 161 low BiEntropy, and red regions represent a disordered phase with a BiEntropy close to one. The regions
 162 are separated by a phase transition where the BiEntropy is intermediate, also captured by the variance
 163 of the BiEntropy (Fig. 3.C and D). The scenario is similar for both signs of b but differs in the details.
 164 The transition (abrupt for $b < 0$, wider for $b > 0$) occurs at a value of σ^* that depends on K (strongly for
 165 $b < 0$, weakly for $b > 0$). The transition widens when K decreases (strongly for $b > 0$). At high K , i.e.
 166 when each neuron is connected with many, there seems to be an asymptotic value for σ^* (or b , indicated on
 167 the upper part of the plots), which is different for $b > 0$ and $b < 0$ (Calvet u. a., 2023). For $K = 2$, the
 168 disordered phase never reaches a BiEntropy of 1, and for $K = 1$ the reservoir is always in its ordered phase
 169 (Bertschinger und Natschläger, 2004).

170 In Fig. 4, we plot the statistics of attractors for reservoirs with $K = 16$ (upper panel), $K = 8$ (middle),
 171 and $K = 4$ (lower), as a function of the balance b . This time $|\sigma^*$ is reported in the upper x-axis. The left
 172 column shows the results for $b < 0$ and the right column for $b > 0$. The phase transition is characterized by
 173 going from attractors with essentially no ($b < 0$) or fixed ($b > 0$) activity in the ordered phase, to attractors
 174 being all irregulars in the disordered phase, with cyclic attractors showing up at the transition. In all plots,
 175 we report the non-zero BiEntropy variance (highlighted by light-grey hatching) to indicate the critical
 176 region (Calvet u. a., 2023). This transition region is clearly defined for $K = 16$, widens for $K = 8$ and
 177 becomes very different for $K = 4$. When $b < 0$, there is a transition region around $b \sim -0.7$ (gray hashed
 178 region) and a re-entrance of the critical region (orange hatching in Fig. 4.E). Indeed, for b between -0.7 and
 179 -0.08 (σ^* between -10 and -2) all attractors are irregular, and cyclic ones reappear for a balance closer to
 180 zero. For $K = 4$ and $b > 0$ the phase transition is never complete, there is no fully disordered phase. Lastly,
 181 near $b = 0$, the attractor statistics are very close from one sign to the other. For example, with $K = 16$ and
 182 $K = 8$ we observe an horizontal line for chaotic attractors, while for $K = 4$, the statistics of cyclic and
 183 irregular attractors closely match on both sides, a fact that is even more visible in the results of Sec. 3.2.1
 184 when varying N .

185 Regarding the control parameter shift from σ^* to b , the phase transition appears inflated in b , as indicated
 186 by the dot positions, particularly for $b < 0$. These positions are generated on an evenly spaced logarithmic
 187 scale in σ^* . The irregular regime is notably compressed, demonstrated by the re-entrant critical region (refer
 188 to Fig. 4.E), spanning from 2.10^1 to 10^3 . This observation suggests that the dynamics remain relatively

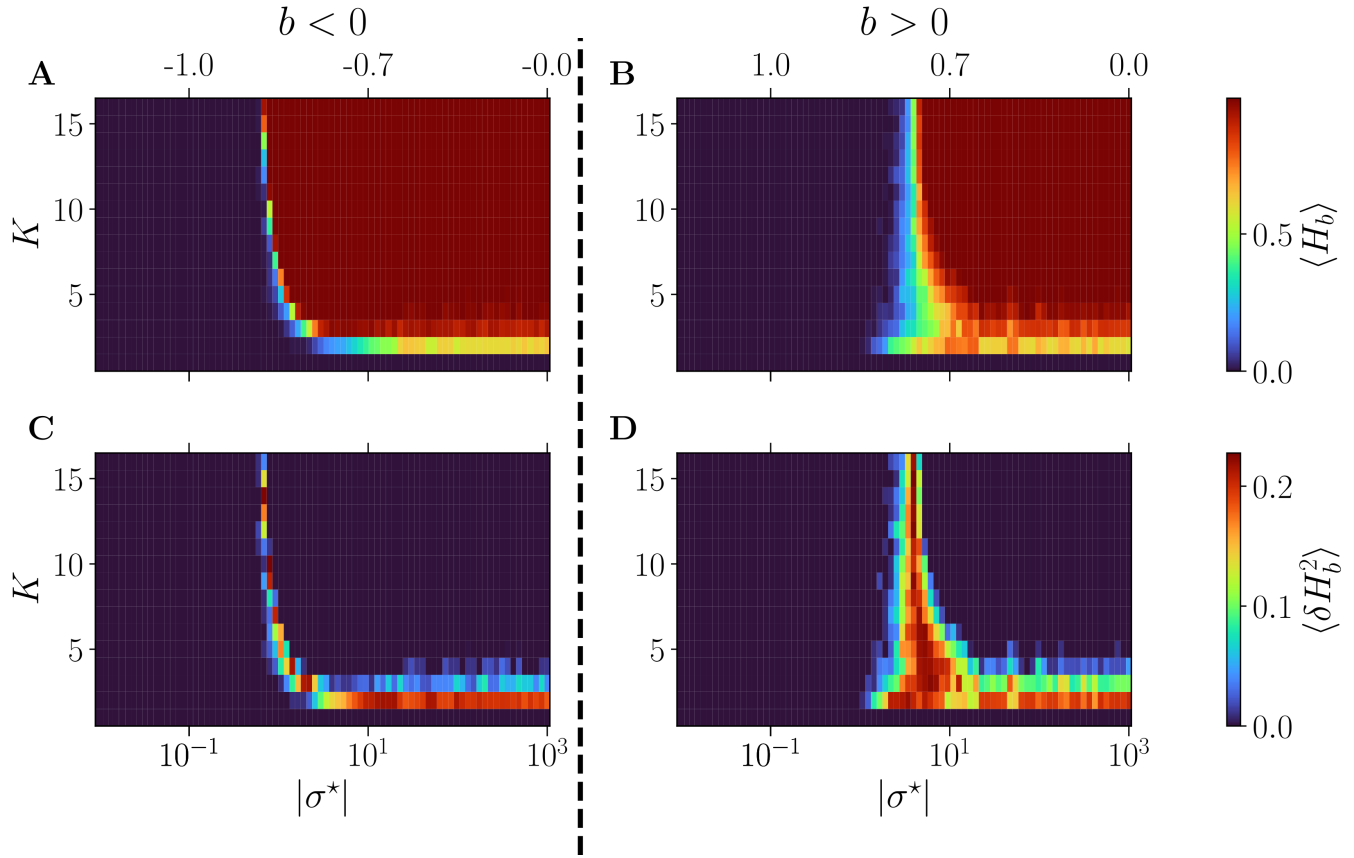


Figure 3. Dynamics of free evolving reservoirs as controlled by the connectivity degree K (y-axis) and $|\sigma^*|$ (x-axis). The upper x-axis displays the corresponding b values, for $b < 0$ (A and C), and $b > 0$ (B and D). The BiEntropy is computed on the steady activities of 100 reservoirs per couple (K, σ^*) . (A and B): The upper row displays the average BiEntropy of the steady state activities (upper left colormap). (C and D): The lower row shows the variance of BiEntropy over reservoirs (bottom left colormap).

189 consistent despite significant variations in the weight distribution parameter. In line with (Metzner und
190 Krauss, 2022; Calvet u. a., 2023), we make the case that underlying b is what is driving the dynamics of
191 these reservoirs. As such, in the rest of the article, we use b as a reference for all further investigations.

192 In conclusion, K has a strong influence on the dynamics of the network. For large values of K , a variety
193 of attractors can be found only in a narrow region of b (σ^*), which is different for both signs of the balance.
194 In contrast, for lower values of K , the co-existence of several attractors is found over a very wide range of
195 σ^* which corresponds to the region where b is small, positive or negative.

196 3.1.2 Impact of the connectivity degree and balance on performance

197 In Fig. 5, we show the performance of the reservoirs for memory tasks as a function of the control
198 parameter b ($|\sigma^*|$ upper x-axis). Five difficulties are operated, with δ varying from -2 to -18 . The left
199 column comprises reservoirs with a negative balance and the right column with a positive one. We show
200 the results for $K = 16$ (upper row), $K = 8$ (middle), and $K = 4$ (bottom).

201 For each value of the delay, reservoirs perform better at low K , and show good performance over a
202 broader range of b . Similar observations have been reported for other tasks (Büsing u. a., 2010). The balance
203 for which performance is best b_{opt} (dotted gray line) strongly depends on K : this is the most visible for
204 $b < 0$ and $\delta = -18$ (the most difficult task), where b_{opt} goes from almost -1 for $K = 16$, to almost 0

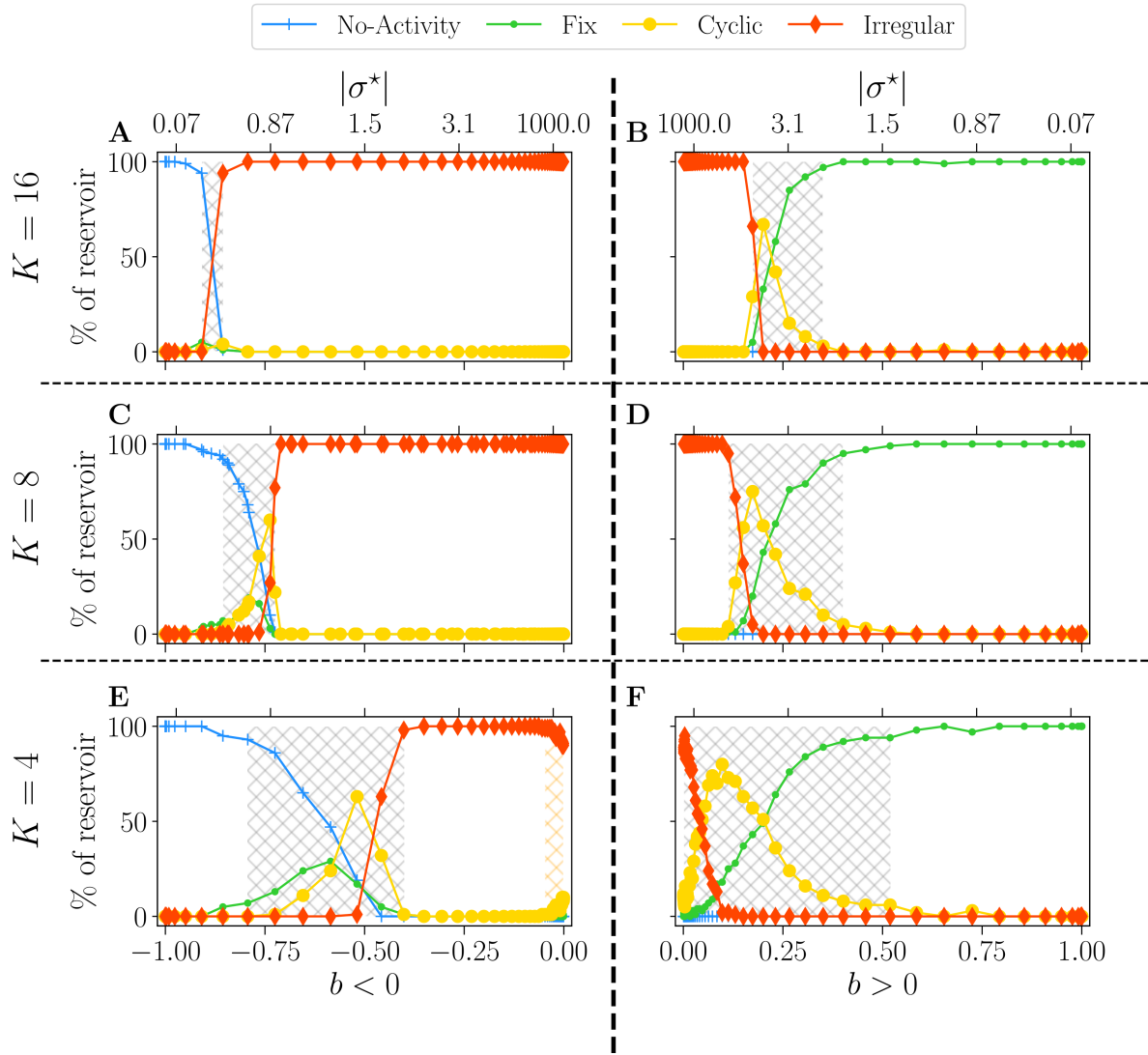


Figure 4. Attractor statistics of free-evolving RBN reservoirs, controlled by K (rows), and the balance b (x-axis). The upper x-axis represents the corresponding $|\sigma^*|$ values, for $b < 0$ (**A**, **C**, **E**), and $b > 0$ (**B**, **D**, **F**). All reservoirs are of size $N = 10000$. Each steady activity signal is classified into one of the four categories of attractors: no-activity (+), fix (•), cyclic (○), irregular (◊). The statistics of attractors are computed over 100 reservoirs run once (y-axis). Results are shown for $K = 16$ (**A** and **B**), $K = 8$ (**C** and **D**), and $K = 4$ (**E** and **F**). The light-gray hatched areas represent the critical regions (Calvet u. a., 2023), defined as the region of non-zero BiEntropy variance; the threshold is chosen to 0.0001. In **E**, the orange hatched area represents a region of re-entrance of criticality with non-zero BiEntropy variance, distinct from the critical region. All hatched areas are computed from the data shown in Fig. 3.C and **D**.

for $K = 4$ (see Tab. 1). For other values of δ the effect is less pronounced but clearly always present. For $b > 0$ the same phenomenon appears and b_{opt} shifts from ~ 0.2 for $K = 16$, to ~ 0 for $K = 4$. Thus, the asymmetry between $b > 0$ and $b < 0$ fades as K decreases. For $K = 4$, the optimal balance, whether positive or negative, is almost zero, i.e., it corresponds to an almost perfect balance between excitation and inhibition. However, notes that performance drops abruptly for $b = 0$: the unbalance, even very small, is essential.

In the prediction task (Fig. 6), a similar trend is observed: as K decreases, the high-performing region shifts towards b values close to zero. Furthermore, the range of b values within the high-performing region

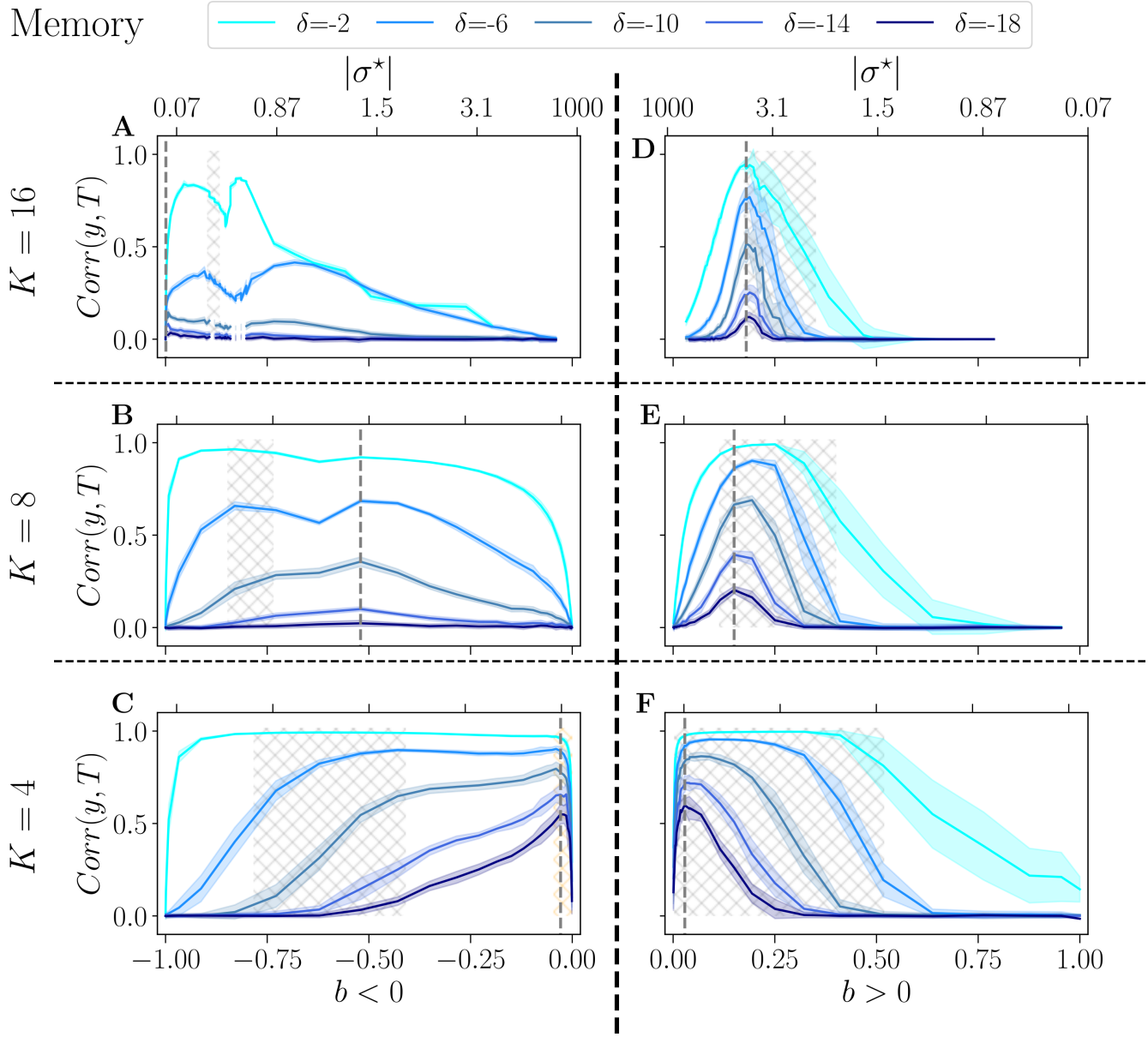


Figure 5. Performance of RBN reservoirs in the memory task of white-noise signals, for various δ , the higher in absolute, the more difficult the task. The correlation between the target and the output (y-axis), is plotted as a function of the control parameter b (x-axis), for a positive balance (**A, B, C**), and a negative balance (**D, E, F**). The upper x-axis represents the corresponding $|\sigma^*|$ values. The solid lines represent the average over 20 reservoirs, higher values signify better performance, while the shaded area represents one standard deviation. (**A** and **E**): the upper row displays $K = 16$, the middle row (**C** and **F**) $K = 8$, and bottom row (**D** and **G**) $K = 4$. The light-gray hatched areas represent the critical regions of BiEntropy variance above a threshold of 0.0001, and the dotted gray lines represent the optimal balance b_{opt} in the most difficult task.

213 is also broader. Still, for $K = 4$, our task may not be sufficiently challenging for the reservoirs, since at
 214 b_{opt} , the three values of τ give very close results. When $b < 0$, the critical region (gray hashed area) does
 215 not align well with the performance peaks, and this discrepancy is even more pronounced for lower $K = 4$.
 216 The peak of performance is still within the orange-hashed region, indicative of re-entrant criticality. In
 217 the case where $b > 0$, in line with previous work (Calvet u. a., 2023), the variance is exceptionally high,

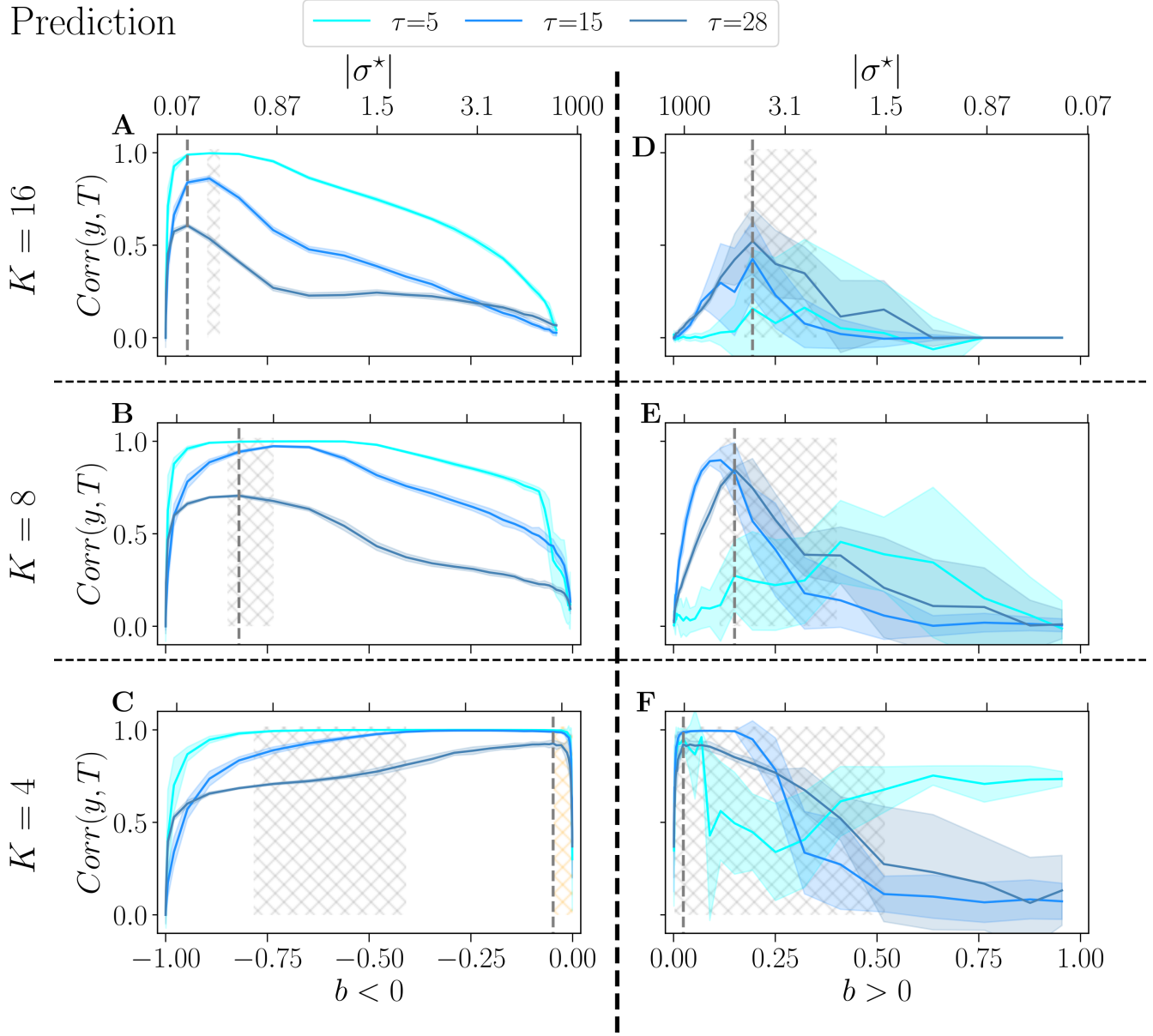


Figure 6. Performance of RBN reservoirs in the prediction task of Mackey-Glass time series, for various τ , the higher, the more complex the signal. The correlation between the target and the output (y-axis), is plotted as a function of the control parameter b (x-axis), for a positive balance (A, B, C), and a negative balance (D, E, F). The upper x-axis represents the corresponding $|\sigma^*|$ values. The solid lines represent the average over 20 reservoirs, higher values signify better performance, while the shaded area represents one standard deviation. (A and E) $K = 16$, with similar result to (Calvet u. a., 2023), (C and F) $K = 8$, and (D and G) $K = 4$. As in the previous figure, the light-gray hashed areas represent the phase transition region, and the dotted gray lines represent the optimal balance b_{opt} in the most difficult task.

218 especially for simpler signals $\tau = 5$ and $\tau = 15$. Surprisingly, for $K = 16$ and $K = 4$, reservoirs perform
219 better at the complex task than at the simpler task $\tau = 5$.

220 Trying to relate criticality with peak performance, we observe that if there is a link between the two, it is
221 rather loose. For $b < 0$ the region of best performance is much broader than the critical region, indicated as
222 hatched gray areas. In many cases, b_{opt} does not lie within the critical region. For $b > 0$, criticality and
223 optimal performance seem more correlated, as optimal performance is usually obtained within the critical

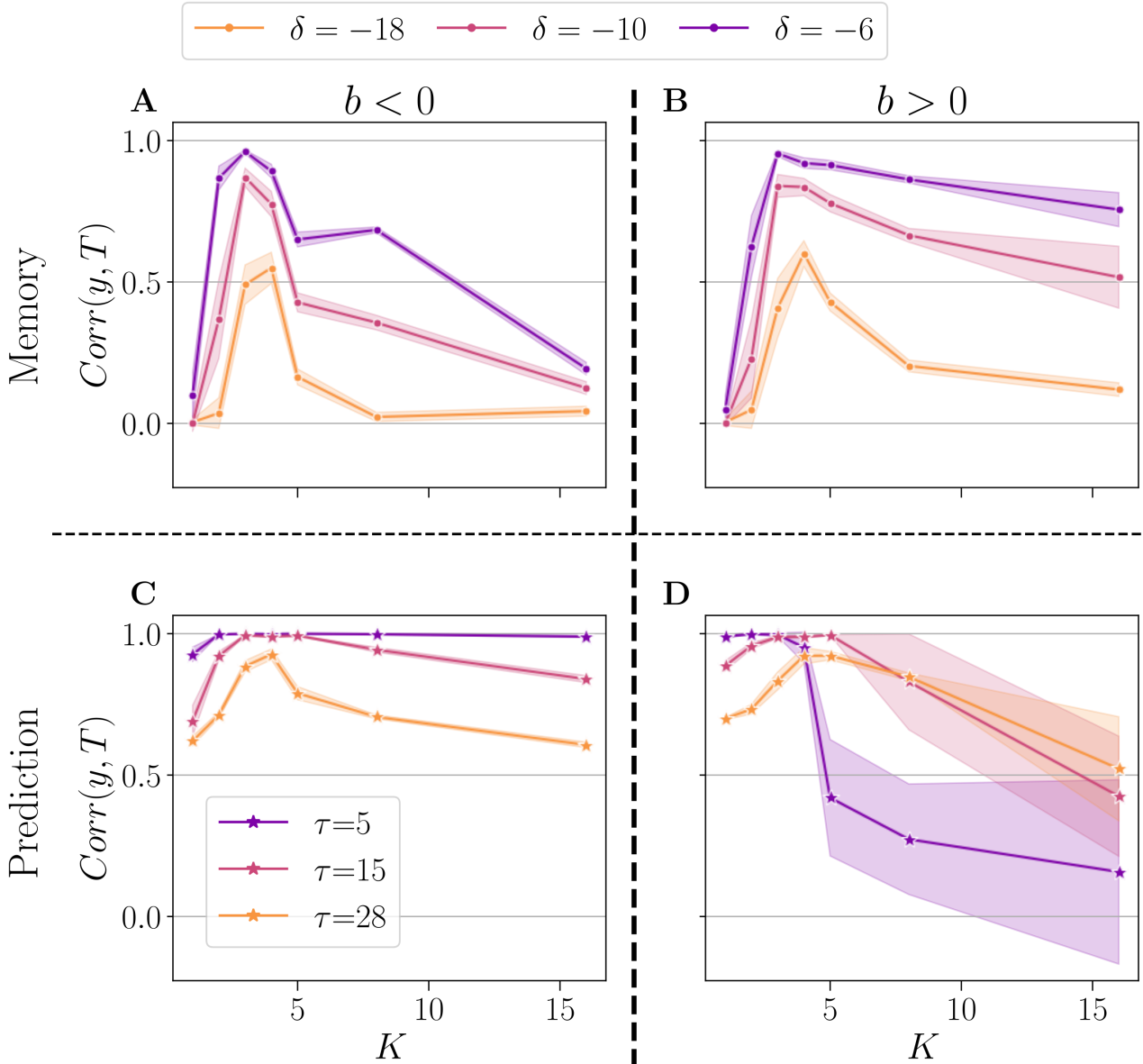


Figure 7. Summary of performance for various connectivity degrees K , in the memory (**A** and **B**) and the prediction (**C** and **D**) tasks. For both $b < 0$ (left panel), and $b > 0$ (right panel). For each value of K , we selected the b_{opt} value giving the highest average performance, in the most difficult task ($\delta = -18$ for memory, and $\tau = 28$ for prediction). We plot the performance (higher is better) of reservoirs $Corr(y, T)$ (y-axis), plotted as a function of K (x-axis). The solid line represents the average over 20 reservoirs (generated with the same b_{opt} and K value), and the shaded area represents one standard deviation. Performance is shown for various δ in the memory task (**A** and **B**), and τ in the prediction (**A** and **B**).

224 region. However, focusing on $K = 4$, $b < 0$ and the hardest memory task (Fig. 5C), there is a striking
 225 difference between criticality and optimal performance: performance is almost zero in the critical region
 226 while it peaks in the region of re-entrance observed in the dynamics of the free running reservoirs, indicated
 227 in Fig. 5C as an orange hatched area. Both regions show a variety of attractors, but only one corresponds to
 228 good performance.

229 To conclude, in Fig. 7, we show a summary of the best performance in the memory (upper panel), and
 230 prediction (lower panel). In the plot, each dot represents the average over 20 reservoirs obtained with the

231 same connectivity parameters (N , K , b_{opt}), where b_{opt} is the value that maximizes the average performance
232 at the most difficult setting of each task ($\delta = -18$ and $\tau = 28$), see Tab. 1 and Tab. 2. As previously, we
233 separated the case $b < 0$ (left panel) and $b > 0$ (right panel). We compare the performance for $K = 1$ up to
234 16.

235 For all tasks, we note that the highest performances are consistently achieved with $K = 3$ and $K = 4$,
236 irrespective of whether b is positive or negative. However, the optimal value of K exhibits some task
237 dependency. In the memory task, for the more challenging task ($\delta = -18$), $K = 4$ yields the best
238 performance, despite $K = 3$ occasionally outperforming less demanding tasks. This suggests that the
239 optimal K may depend on the complexity of the task at hand. The sign of b has no discernible impact on
240 the optimal K , however, it is observed that the performance for higher K values is superior when $b > 0$, in
241 line with (Calvet u. a., 2023).

242 In the prediction task, again, the most challenging setup ($\tau = 28$) shows $K = 4$ as the optimal value,
243 irrespective of the sign of b . In general, the reservoir-to-reservoir variance is very small for $b < 0$. As
244 previously observed, for higher K , we observe a significant reservoir variability, and this time, the
245 performance is higher when $b < 0$.

246 Taken together, these findings suggest that once an optimal value for K is selected, the system's
247 performance becomes mainly insensitive to the sign of the balance b , even though the optimal K can be
248 dependent on the task at hand.

249 3.1.3 Discussion

250 In line with (Calvet u. a., 2023), for a positive balance, the critical region is reasonably aligned with the
251 performing region, for all tested K . Yet our findings somewhat challenge the idea that the edge of chaos is
252 always optimal for computation, as it does not necessarily overlap with the region of best performance.
253 This is especially visible in the memory tasks and reservoirs with a negative balance. Indeed, for $K = 4$,
254 the re-entrant region provides the best reservoirs, while being very far from criticality.

255 By looking at dynamics, one might wonder if this re-entrant region of attractor diversity ($b < 0$) does
256 not belong to the critical region of the positive side, which, by shifting towards the left, overlaps on the
257 negative sign. On the other hand, we observe a drastic dip in performance with both signs around $b = 0$.
258 This suggests that a breaking of symmetry is at play Goldenfeld (2018), acting as a crucial driver for
259 performance while being surprisingly imperceptible in the dynamic.

260 Regarding reservoir design, we show that the optimal excitatory/inhibitory balance is intricately tied
261 to the number of connections. For a high number of connections, a pronounced asymmetry is observed
262 depending on whether there is a majority of inhibition or excitation.

263 However, when $K = 4$, the optimal b value is almost identical and closely balanced between excitation
264 and inhibition, regardless of whether b is positive or negative. Consequently, the dynamics of reservoirs are
265 nearly identical for both positive and negative b , resulting in similar performance outcomes. The task of
266 choosing the optimal b_{opt} becomes much simpler, as the asymmetry fades away.

267 3.2 The interplay between reservoir size and connectivity degree

268 This section studies the joint effect of the reservoir size N (=100, 1000, 10000) and K , in relation to b .
269 We show that N has a comparable impact on the dynamics as K , but also impacts asymmetrically around b
270 the performance in tasks.

271 3.2.1 Impact of reservoir size and connectivity degree on dynamics

272 In Fig. 8, we set $K = 4$ and present the attractor statistics over b for three different values of N :
 273 $N = 10000$ (upper panel), $N = 1000$ (middle panel), and $N = 100$ (lower panel). We analyze these values
 274 in two cases, $b < 0$ (left panel) and $b > 0$ (right panel).

275 From our observations, it is evident that reducing N leads to a decrease in the complexity of the attractors,
 276 as indicated by the reduction of irregular attractors. In the case of $b < 0$ and as N decreases, the re-entrant
 277 region (orange hashed area) observed with $N = 10000$ (Fig. 8.A) merges with the critical one (gray hashed
 278 area) for $N = 1000$ (Fig. 8.C), resulting in a spike of irregular attractors and eventually leaving room for
 279 predominantly cyclic ones as $N = 100$ (Fig. 8.C).

280 Contrarily, for $b > 0$ and $N = 1000$, this spike or irregular attractor is missing, and the critical phase
 281 is largely dominated by cyclic attractors, with only a few fixed and irregular ones. Interestingly, when
 282 $N = 100$, both signs yield very similar results, with no irregular attractors at all. This observation
 283 underscores the impact of N on the nature and complexity of the attractors.

284 Lastly, when discussing Fig. 4, we briefly mentioned the continuity in attractor statistics as going from a
 285 negative to a positive balance. This fact is even more salient in Fig. 8. Statistics of attractors closely match
 286 on both sides, reinforcing the picture that the critical region can span both signs, at least from the dynamic
 287 lens.

288 3.2.2 Impact of reservoir size and connectivity degree on performance

289 Results for the memory task and prediction are respectively displayed in Fig 9 and Fig. 10. We tested
 290 the performance for $K = 4$ (upper panel), $K = 8$ (middle) and $K = 16$ (bottom). Reservoirs with $b < 0$
 291 are displayed in the left panel and $b > 0$ in the right panel. We compare the performance for three distinct
 292 values of N : $N = 10000$ (green curves), $N = 1000$ (orange curves), and $N = 100$ (blue curves). As in the
 293 previous Sec. 3.1.2, performance is shown for b_{opt} , established for the most difficult setting in each task
 294 ($\delta = -18$ and $\tau = 28$).

295 In the memory task, as expected, reducing the number of neurons diminishes the reservoirs's memory
 296 capacity, and the more difficult the task, the lower the performance. In addition, decreasing the reservoir
 297 size generally increases the reservoir-to-reservoir variance, as indicated by the larger error bars, even
 298 though this is not always the case, especially when performance is already low.

299 The number of neurons exerts a greater influence when K is lower. Indeed, for $K = 4$, we observe a
 300 significant disparity between all three N values across all difficulty levels (δ). Surprisingly, for higher K ,
 301 and especially when $b < 0$, performances for $N = 1000$ and $N = 10000$ are relatively comparable, and
 302 increasing the reservoir size is not improving performance, especially for tasks requiring longer memory.
 303 As previously noted, when $K = 4$, performance is similar regardless of whether b is positive or negative, a
 304 finding that is now corroborated across all tested N values.

305 It appears that K has minimal influence when $N = 100$, as reservoirs perform similarly regardless of K .
 306 The same holds true for both positive and negative b , which their identical dynamics profiles might explain.
 307 This suggests that, for low neuron counts, the system's dynamics and performance are more strongly
 308 influenced by the balance parameter b than by the number of connections K .

309 In the prediction task, we observe some surprising trends. Notably, having a higher N is not always
 310 advantageous, as the optimal N appears to depend on both the task and the control parameter.

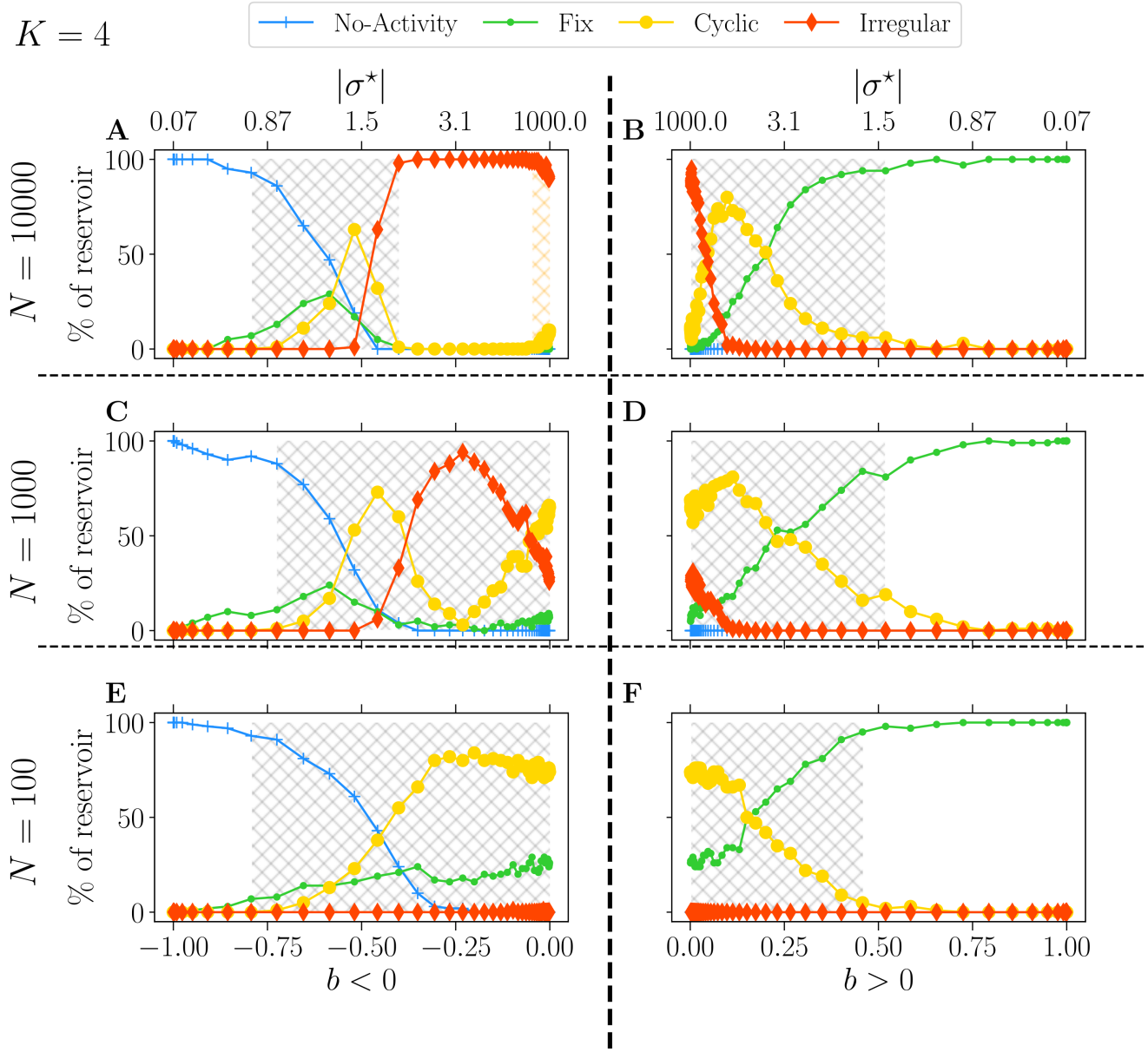


Figure 8. Attractor statistics of free-evolving RBN reservoirs for fixed $K = 4$, with $N = 10000$ (**A** and **B**), $N = 1000$ (**C** and **D**), and $N = 100$ (**E** and **F**). Statistics of attractors over 100 reservoirs run once (y-axis) versus b (x-axis). The upper x-axis displays the corresponding $|\sigma^*|$, both for $b < 0$ (left panel) and $b > 0$ (right panel). Each activity signal is classified into one of the six categories of attractors: extinguished, fixed, cyclic, and irregular, defined in methodology Sec. 2.3. The light-gray hatched areas represent the critical regions defined; the threshold is chosen to 0.0001. In **A**, the orange hatched area represents the region of re-entrance of criticality with non-zero BiEntropy variance.

311 Firstly, for $b < 0$, the performance profile is similar to that in the memory task: higher N yields better
 312 performance, and performance decreases with increasing task difficulty (τ). However, the performances of
 313 $N = 10000$ and $N = 1000$ are closer to each other and significantly higher than that of $N = 100$, which
 314 again remains unaffected by K .

315 Secondly, for $b > 0$, the value of K strongly influences the relationship between performance and
 316 reservoir size. With $K = 4$, the performance profile is similar to that for $b < 0$: performance decreases
 317 monotonically with τ and N . However, for $K = 8$ and especially for $K = 16$, we observe some

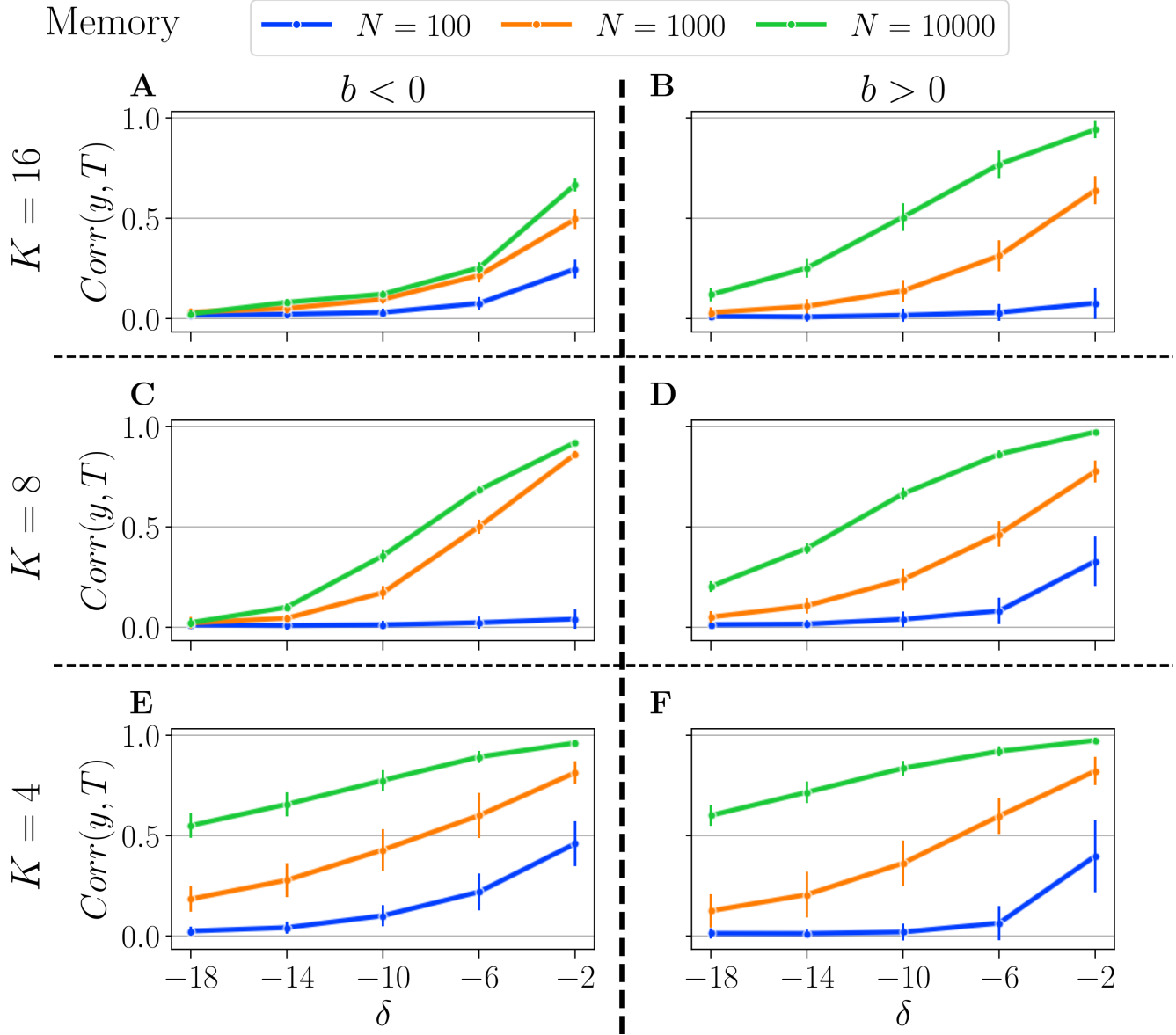


Figure 9. Summary of performance in the memory tasks, for various connectivity degrees K , and size of the reservoirs N : for $N = 10000$ (green curves), $N = 1000$ (orange curves), and $N = 100$ (blue curves). $K = 16$ (**A** and **B**), $K = 8$ (**C** and **D**), $K = 4$ (**E** and **F**). $b < 0$ (left column), and $b > 0$ (right column). Solid lines represent the average over all reservoirs generated with the same reservoir (N, K, b_{opt}), and the error bar represents one standard deviation. As explained in Sec. 3.1.2, b_{opt} is obtained by selecting the balance that gives the best average performance at the most difficult setting in each respective task.

318 unexpected results. Smaller reservoirs ($N = 1000$) can outperform larger ones ($N = 10000$) in some tasks.
 319 This phenomenon is even more pronounced for higher K , as the orange line (representing $N = 1000$)
 320 consistently outperforms the green line (representing $N = 10000$) across all tested tasks.

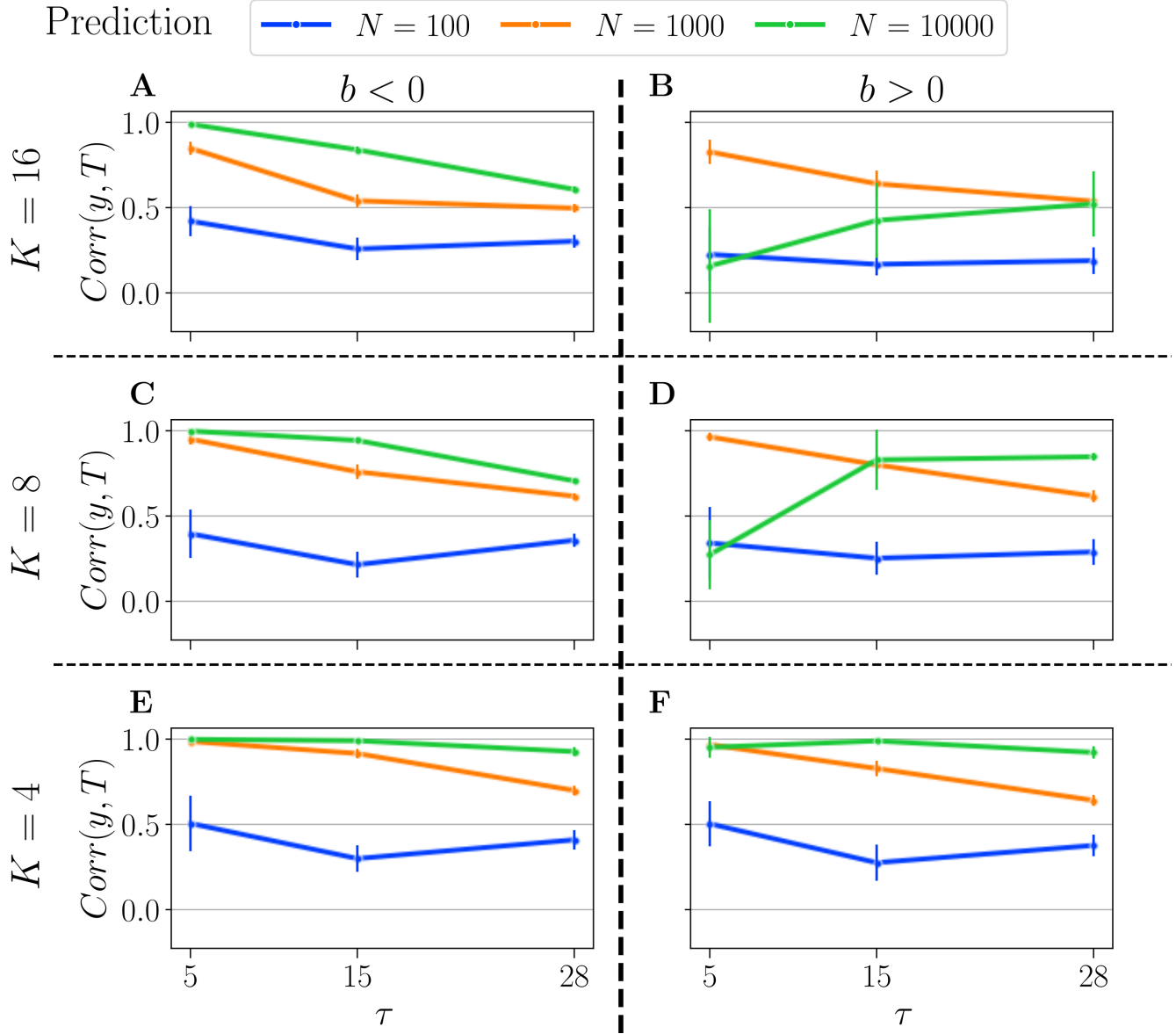


Figure 10. Summary of performance in the prediction tasks, for various connectivity degrees K , and size of the reservoirs N : for $N = 10000$ (green curves), $N = 1000$ (orange curves), and $N = 100$ (blue curves). $K = 16$ (A and B), $K = 8$ (C and D), $K = 4$ (E and F). $b < 0$ (left column), and $b > 0$ (right column). For more information on the plots, see the caption of Fig. 9.

4 DISCUSSION

Our study reveals that the edge of chaos, or the critical region, does not consistently align with the peak performance region (Gallicchio, 2020), and this alignment is contingent upon the sign of excitatory-inhibitory balance b . For $b > 0$, as previously observed (Calvet u. a., 2023), the critical region coincides with the highest performance. However, for $b < 0$, the region of optimal performance does not coincide with the critical region when the connectivity degree K is optimally selected. Instead, supplanting the disordered phase, a re-entrance of the critical region is observed, indicated by an increased attractor diversity, which surprisingly aligns with the best-performing region. This insight suggests that the attractor

328 dynamics can be utilized to identify the region of interest for the design or reservoirs, and this also holds
329 for $b > 0$ and its identified critical region (Calvet u. a., 2023).

330 In terms of the interplay between b and the connectivity degree K , our research shows that a carefully
331 selected K ($K = 4$) renders the sign of b irrelevant, as the optimal b becomes $\pm\epsilon$ with ϵ very small.
332 This suggests that the optimal balance is near, but not at, perfect symmetry, even though $b \rightarrow 0$ results
333 in zero performance. In statistical physics, it is well known that symmetry breaking induces critical
334 phase transitions (Goldenfeld, 2018), and our findings suggest that symmetry breaking in the balance
335 of excitatory-inhibitory synapses is crucial for achieving optimal performance. Refining initial literature
336 (Bertschinger und Natschläger, 2004; Snyder u. a., 2013; Burkow und Tufte, 2016; Echlin u. a., 2018), the
337 highest-performing region is characterized by a preponderance of irregular attractors within the disordered
338 region.

339 To understand this, one can consider what happens when σ^* tends to infinity. This can be achieved in
340 two ways: first, when the standard deviation of the weight σ is fixed while the mean weights $\mu \rightarrow 0$, and
341 second, when μ is fixed while $\sigma \rightarrow \infty$. The first case has been covered in other works (Bertschinger und
342 Natschläger, 2004; Büsing u. a., 2010) and shows the importance of tuning the scaling of the input weights
343 with the recurrent weight statistics (Burkow und Tufte, 2016). In the present work, however, the second
344 option is considered, as the mean weights is fixed, and σ increases to higher values. As such, b approaches
345 zero, which results in a symmetry between excitation and inhibition but with increasingly higher synaptic
346 weights (in absolute value). Consequently, each neuron receives equal excitatory and inhibitory recurrent
347 inputs, and since the input weights are kept constant, the external input becomes insignificant. Finally, since
348 neurons have a zero threshold, they have a 50% probability of spiking, leading to a random spike train.
349 Therefore, it is not surprising to observe a performance dip as $\sigma \rightarrow \infty$ ($b \rightarrow 0$) since the reservoir activity
350 becomes independent of the input. However, what requires further investigation is the unexpected drastic
351 performance increase when this symmetry is slightly broken as $b = \pm\epsilon \sim 0.03$ (roughly corresponding to
352 a 6% difference between excitatory and inhibitory synapses).

353 These findings highlight the critical role of K in determining other control parameters. Firstly, the optimal
354 number of connections ($K = 4$) eliminates the performance asymmetry, significantly simplifying the
355 parameter b selection. Secondly, consistent with previous studies, N generally enhances performance, but
356 this is only true for optimal $K = 4$ values, particularly in the prediction task, where smaller reservoirs
357 occasionally outperform larger ones. Additionally, the performance gain obtained by K is significant only
358 when the reservoir size is sufficiently large. For instance, with reservoirs of size $N = 100$, K had close to
359 no effect on the best performance. However, optimally choosing K becomes key to obtaining a gain in
360 performance when increasing the size.

361 Our work reveals a complex interplay between the topology and weights parameters, but assuming a
362 reservoir of sufficient size ($N \geq 1000$), K acts as a pivotal control parameter by greatly simplifying the
363 way parameters interact with each other. When K is optimal, then N must be maximized, and b can be
364 chosen very close to zero but finite, and of any sign.

5 FUTURE WORK

365 Understanding the relationship between dynamics and performance is crucial for simplifying reservoir
366 design (Bertschinger und Natschläger, 2004; Krauss u. a., 2019b,a; Metzner und Krauss, 2022; Calvet u. a.,
367 2023). Our study advances this understanding but reveals a more intricate relationship than anticipated.
368 Specifically, performance was found to be highly sensitive to symmetry breaking in the excitation-inhibition

369 balance, while the metrics used to probe the dynamics were completely unaware of the symmetry. Future
370 research could investigate the relationship between the optimal balance and other dynamic-probing metrics,
371 including spatial and temporal correlation (Metzner und Krauss, 2022), and possibly topology (Kinoshita
372 u. a., 2009; Masulli und Villa, 2015). For instance, it could be hypothesized that the longest neural pathways
373 in the random graph become available for information transmission only at $b = \pm\epsilon$, which could explain
374 why optimal performance necessitates a breaking of symmetry in the balance.

ACKNOWLEDGEMENT

375 The authors are grateful to Lucas Herranz for carefully reviewing the manuscript. They also want to thank
376 their colleagues at NECOTIS for their helpful feedback and productive discussions during the research
377 process.

CONFLICT OF INTEREST STATEMENT

378 The researchers affirm that their study was carried out without any affiliations or transactions that could
379 give rise to a possible conflict of interest.

AUTHOR CONTRIBUTIONS

380 This article is a collaboration between EC, BR, and JR. EC conducted the research, developed the model,
381 collected and analyzed data, and wrote the manuscript. BR and JR provided guidance, perspective, and
382 contributed to the manuscript. All authors approved the final version.

FUNDING

383 This work was supported by the CRSNG/NSERC, the Canada Research Chair Program, NSERC, and
384 CFREF.

CODE AND DATA AVAILABILITY

385 The study used custom code and data from a repository created by the author (?).

REFERENCES

- 386 [Bertschinger und Natschläger 2004] BERTSCHINGER, Nils ; NATSCHLÄGER, Thomas: Real-Time
387 Computation at the Edge of Chaos in Recurrent Neural Networks. In: *Neural Computation* 16
388 (2004), 7, Nr. 7, S. 1413–1436. – URL <https://direct.mit.edu/neco/article/16/7/1413-1436/6890>. – ISSN 0899-7667
- 390 [Bianchi u. a. 2016] BIANCHI, Filippo M. ; LIVI, Lorenzo ; ALIPPI, Cesare: Investigating
391 echo state networks dynamics by means of recurrence analysis. In: *IEEE transactions
392 on neural networks and learning systems* 29 (2016), 1, Nr. 2, S. 427–439. –
393 URL <http://www.ncbi.nlm.nih.gov/pubmed/28114039> <http://arxiv.org/abs/1601.07381> <http://dx.doi.org/10.1109/TNNLS.2016.2630802>. – ISSN 2162-2388
- 395 [Burkow und Tufte 2016] BURKOW, Aleksander V. ; TUFTE, Gunnar: *Exploring Physical Reservoir
396 Computing using Random Boolean Networks*, Norwegian University of Science and Technology - NTNU,
397 Dissertation, 2016. – URL <http://hdl.handle.net/11250/2417596>

- 398 [Büsing u. a. 2010] BÜSING, Lars ; SCHRAUWEN, Benjamin ; LEGENSTEIN, Robert: Connectivity,
399 dynamics, and memory in reservoir computing with binary and analog neurons. In: *Neural Computation*
400 22 (2010), Nr. 5, S. 1272–1311. – ISSN 08997667
- 401 [Calvet u. a. 2023] CALVET, Emmanuel ; ROUAT, Jean ; REULET, Bertrand: Excitatory/inhibitory
402 balance emerges as a key factor for RBN performance, overriding attractor dynamics. In: *Frontiers*
403 in *Computational Neuroscience* 17 (2023), 8. – URL <https://www.frontiersin.org/articles/10.3389/fncom.2023.1223258/full>. – ISSN 1662-5188
- 405 [Cherupally 2018] CHERUPALLY, Sai K.: Hierarchical Random Boolean Network Reservoirs / Portland
406 State University. Portland, OR, 1 2018. – Forschungsbericht. – URL <https://archives.pdx.edu/ds/psu/25510>
- 408 [Cramer u. a. 2020] CRAMER, Benjamin ; STÖCKEL, David ; KREFT, Markus ; WIBRAL, Michael ;
409 SCHEMMEL, Johannes ; MEIER, Karlheinz ; PRIESEMANN, Viola: Control of criticality and computation
410 in spiking neuromorphic networks with plasticity. In: *Nature Communications* 11 (2020), Nr. 1. – URL
411 <https://doi.org/10.1038/s41467-020-16548-3>. – ISSN 20411723
- 412 [Croll 2014] CROLL, Grenville J.: BiEntropy – the Measurement and Algebras of Order and Disorder
413 in Finite Binary Strings. In: ST ANDREWS, UK) John C Amson (University of (Hrsg.) ; CHICAGO,
414 USA) Louis H Kauffman (University of Illinois at (Hrsg.): *Scientific Essays in Honor of H Pierre*
415 *Noyes on the Occasion of His 90th Birthday*. Series on. Word Scientific, 1 2014, S. 48–64. – URL
416 http://www.worldscientific.com/doi/abs/10.1142/9789814579377_0004
- 417 [Echlin u. a. 2018] ECHLIN, Moriah ; AGUILAR, Boris ; NOTARANGELO, Max ; GIBBS, David ;
418 SHMULEVICH, Ilya: Flexibility of Boolean Network Reservoir Computers in Approximating Arbitrary
419 Recursive and Non-Recursive Binary Filters. In: *Entropy* 20 (2018), 12, Nr. 12, S. 954. – URL
420 <http://www.mdpi.com/1099-4300/20/12/954>. – ISSN 1099-4300
- 421 [Gallicchio 2020] GALLICCHIO, Claudio: Sparsity in Reservoir Computing Neural Networks. In: *2020*
422 *International Conference on INnovations in Intelligent SysTems and Applications (INISTA)*, IEEE,
423 8 2020, S. 1–7. – URL <https://ieeexplore.ieee.org/document/9194611/>. – ISBN
424 978-1-7281-6799-2
- 425 [Glass und Hill 1998] GLASS, L. ; HILL, C.: Ordered and disordered dynamics in random networks. In:
426 *Europhysics Letters (EPL)* 41 (1998), 3, Nr. 6, S. 599–604. – URL <https://iopscience.iop.org/article/10.1209/epl/i1998-00199-0>. – ISSN 0295-5075
- 428 [Goldenfeld 2018] GOLDENFELD, Nigel: *Lectures on Phase Transitions and the Renormalization*
429 *Group*. CRC Press, 3 2018. – 1–394 S. – URL <https://www.taylorfrancis.com/books/9780429962042>. – ISBN 9780429493492
- 431 [Hajnal und Lörincz 2006] HAJNAL, Márton A. ; LÖRINCZ, András: Critical echo state networks. In:
432 *Lecture Notes in Computer Science (including subseries Lecture Notes in Artificial Intelligence and*
433 *Lecture Notes in Bioinformatics)* 4131 LNCS (2006), Nr. September 2006, S. 658–667. – ISBN
434 3540386254
- 435 [Jaeger 2005] JAEGER, Herbert: A tutorial on training recurrent neural networks
436 , covering BPPT , RTRL , EKF and the ” echo state network ” approach. In:
437 *ReVision* 2002 (2005), S. 1–46. – URL <http://www.mendeley.com/catalog/tutorial-training-recurrent-neural-networks-covering-bppt-rtrtl-ekf-echo-sta>
438 ISBN 159
- 440 [Kingma und Ba 2015] KINGMA, Diederik P. ; BA, Jimmy: Adam: A Method for Stochastic Optimization.
441 In: *3rd International Conference for Learning Representations, San Diego*, ICLR, 12 2015. – URL
442 <http://arxiv.org/abs/1412.6980>

- 443 [Kinoshita u. a. 2009] KINOSHITA, Shu-ichi ; IGUCHI, Kazumoto ; YAMADA, Hiroaki S.: Intrinsic
444 properties of Boolean dynamics in complex networks. In: *Journal of Theoretical Biology* 256
445 (2009), 2, Nr. 3, S. 351–369. – URL <https://linkinghub.elsevier.com/retrieve/pii/S0022519308005456>. – ISSN 00225193
- 446
- 447 [Krauss u. a. 2019a] KRAUSS, Patrick ; SCHUSTER, Marc ; DIETRICH, Verena ; SCHILLING, Achim ;
448 SCHULZE, Holger ; METZNER, Claus: Weight statistics controls dynamics in recurrent neural networks.
449 In: *PLOS ONE* 14 (2019), 4, Nr. 4, S. e0214541. – URL <https://dx.plos.org/10.1371/journal.pone.0214541>. – ISBN 1111111111
- 450
- 451 [Krauss u. a. 2019b] KRAUSS, Patrick ; ZANKL, Alexandra ; SCHILLING, Achim ; SCHULZE, Holger ;
452 METZNER, Claus: Analysis of Structure and Dynamics in Three-Neuron Motifs. In: *Frontiers in Computational Neuroscience* 13 (2019), 2, Nr. February, S. 1–6. – URL <https://www.frontiersin.org/article/10.3389/fncom.2019.00005/full>. – ISSN 1662-5188
- 453
- 454 [Legenstein und Maass 2006] LEGENSTEIN, Robert ; MAASS, Wolfgang: What Makes a Dynamical System Computationally Powerful? In: SIMON HAYKIN, Terrence J. Sejnowski John M. (Hrsg.): *New Directions in Statistical Signal Processing*. The MIT Press, 10 2006, S. 127–154. – URL <https://direct.mit.edu/books/book/3805/chapter/124942/6-what-makes-a-dynamical-system-computationally>. – ISBN 9780262256315
- 455
- 456 [Luque und Solé 2000] LUQUE, Bartolo ; SOLÉ, Ricard V.: Lyapunov exponents in random Boolean
457 networks. In: *Physica A: Statistical Mechanics and its Applications* 284 (2000), 9, Nr. 1-4, S. 33–45.
458 – URL <https://linkinghub.elsevier.com/retrieve/pii/S0378437100001849>. – ISSN 03784371
- 459
- 460 [Maass u. a. 2002] MAASS, Wolfgang ; NATSCHLÄGER, Thomas ; MARKRAM, Henry ; MAASS ;
461 NATSCHLAGER ; MARKRAM: Real-time Computing Without Stable States: A New Framework
462 for Neural Computation Based on Perturbations. In: *NEURCOMP: Neural Computation* 14 (2002),
463 Nr. 11, S. 2531–2560. – URL <http://www.ncbi.nlm.nih.gov/pubmed/12433288>. – ISBN
464 0899-7667 (Print) \r0899-7667 (Linking)
- 465
- 466 [Masulli und Villa 2015] MASULLI, Paolo ; VILLA, Alessandro E. P.: The topology of the directed clique
467 complex as a network invariant. In: *SpringerPlus* 5 (2015), 10, Nr. 1, S. 388. – URL <http://arxiv.org/abs/1510.00660> <http://dx.doi.org/10.1186/s40064-016-2022-y> –
468 ISBN 4006401620
- 469
- 470 [Metzner und Krauss 2022] METZNER, Claus ; KRAUSS, Patrick: Dynamics and Information Import in
471 Recurrent Neural Networks. In: *Frontiers in Computational Neuroscience* 16 (2022), 4, Nr. April, S. 1–15.
472 – URL <https://www.frontiersin.org/articles/10.3389/fncom.2022.876315/full>. – ISSN 1662-5188
- 473
- 474 [Natschläger u. a. 2005] NATSCHLÄGER, Thomas ; BERTSCHINGER, Nils ; LEGENSTEIN, Robert: At the
475 edge of chaos: Real-time computations and self-organized criticality in recurrent neural networks. In:
476 *Advances in Neural Information Processing Systems* 17, NeurIPS, 2005. – ISBN 0262195348
- 477
- 478 [Nowshin u. a. 2020] NOWSHIN, Fabiha ; ZHANG, Yuhao ; LIU, Lingjia ; YI, Yang: Recent Advances in
479 Reservoir Computing With A Focus on Electronic Reservoirs. In: *2020 11th International Green and
480 Sustainable Computing Workshops (IGSC)*, IEEE, 10 2020, S. 1–8. – URL <https://ieeexplore.ieee.org/document/9290858/>. – ISBN 978-1-6654-1552-1
- 481
- 482 [Snyder u. a. 2012] SNYDER, David ; GOUDARZI, Alireza ; TEUSCHER, Christof: Finding Optimal
483 Random Boolean Networks for Reservoir Computing. In: *Artificial Life* 13, MIT Press, 7
- 484

- 487 2012, S. 259–266. – URL <https://www.mitpressjournals.org/doi/abs/10.1162/978-0-262-31050-5-ch035>. – ISBN 9780262310505
- 489 [Snyder u. a. 2013] SNYDER, David ; GOUDARZI, Alireza ; TEUSCHER, Christof: Computational
490 capabilities of random automata networks for reservoir computing. In: *Physical Review E* 87 (2013), 4,
491 Nr. 4, S. 042808. – URL <https://link.aps.org/doi/10.1103/PhysRevE.87.042808>.
492 – ISSN 1539-3755
- 493 [Steiner u. a. 2023] STEINER, Peter ; JALALVAND, Azarakhsh ; BIRKHOLZ, Peter: Cluster-Based
494 Input Weight Initialization for Echo State Networks. In: *IEEE Transactions on Neural Networks and*
495 *Learning Systems* 34 (2023), Nr. 10, S. 7648–7659. – URL <https://ieeexplore.ieee.org/document/9705114/>. – ISSN 2162-237X
- 497 [Triefenbach u. a. 2010] TRIEFENBACH, Fabian ; JALALVAND, Azarakhsh ; SCHRAUWEN, Benjamin ;
498 MARTENS, Jean P.: Phoneme recognition with large hierarchical reservoirs. In: *Advances in Neural*
499 *Information Processing Systems 23: 24th Annual Conference on Neural Information Processing Systems*
500 *2010, NIPS 2010*, NIPS, 2010. – ISBN 9781617823800
- 501 [Zhu u. a. 2021] ZHU, Ruomin ; HOCHSTETTER, Joel ; LOEFFLER, Alon ; DIAZ-ALVAREZ, Adrian ;
502 NAKAYAMA, Tomonobu ; LIZIER, Joseph T. ; KUNCIC, Zdenka: Information dynamics in neuromorphic
503 nanowire networks. In: *Scientific Reports* 11 (2021), Nr. 1, S. 1–15. – URL <https://doi.org/10.1038/s41598-021-92170-7>. – ISBN 4159802192

505 *Supplementary Material*

6 TRAINING

506 Both tasks follow the same protocol for training the readout weights:

507 • Reservoirs receive the input u for $D = 2000$ time steps.

508 • We discard the first 500 time steps.

509 • The training is then performed on the subsequent 1500 time steps. We concatenate the reservoir outputs
510 in time, and use the optimization procedure defined in 2.1.511 Each experiment consists in 40 values of σ^* per sign of b , and is performed for three values of $K =$
512 $\{4, 8, 16\}$ and three values of $N = \{100, 1000, 10000\}$. For each value (σ^*, K, N) , 20 reservoirs are
513 randomly generated, and each network is run 5 times with different randomly tossed inputs (i.e., 14, 400
514 simulations). Each training is performed for 4000 epochs (with a total of 57,600,000 training epochs).515 **6.1 The density is not a control parameter**516 Historically, the litterature on RBN studied the connectivity degree K , along with the number of neurons
517 in the reservoir N . It has been shown that RBN reservoirs possess interesting computational properties for
518 very sparse matrices, with at most $K = 25$ connections per neuron, according to (Büsing u. a., 2010). On
519 the other hand, studies in ESN have explored the impact of another parameter, the density d (Hajnal und
520 Lörincz, 2006; Krauss u. a., 2019a; Metzner und Krauss, 2022), which captures how many zeros there are
521 in the adjacency matrix, ranging from zero for no connections, to one for fully connected reservoirs.522 In the context of RBN reservoirs, the density is equal to $d = K/N$. It is worth noting that for the values
523 of K and N used in this study, the corresponding values of d are ridiculously small, ranging from 0,0004
524 to 0.16. This stresses how much the RBN behaves differently since phase transitions occur at a fraction of
525 what is observed in an ESN. It also suggests that K is a more natural choice for the control parameter of
526 the RBN.527 Nonetheless, this is not sufficient to rule out d as a good candidate for control parameters. Recalling that
528 it is in the same fashion that μ and σ were shown to be dependent parameters and $\sigma^* = \mu/\sigma$ was built in
529 (Calvet u. a., 2023). If d is a control parameter, however, then all combinations of K and N leading to the
530 same values of d should provide the exact same dynamics and performance in tasks, as is the case with σ^* .
531 To find if d is indeed a control parameter, we study the dynamics and performance of three couples of K
532 and N giving the same value d :

$$d = K/N = 16/10000 = 8/5000 = 4/2500 = 0.0016$$

533 In Fig. 11, we show the attractor statistics in the three conditions, as a function of b . The first thing we
534 notice is that all three tested conditions give very different attractor profiles. The width and the location of
535 the critical regions are not the same, and the proportion of attractors also greatly varies, with lower K and
536 N giving much more varied dynamics and wider critical regions. It is intriguing that in Fig. 4 and Fig. 8,
537 diminishing K and N results in a somewhat comparable increase in the dynamics variability as well, but if
538 K and N seem related, it is not by their ratio as proposed in the density parameter.

539 In addition, we show in Fig. 12 the performance in memory and prediction of 20 reservoirs selected with
 540 the same b_{opt} values, for each couple (N, K) (for more information on how these plots are obtained see
 541 Sec. 3.1.2). Following the dynamics analysis, even though each couple (N, K) possesses the same density,
 542 the performance varies.

543 When considering $b < 0$, smaller K consistently provides higher performance in all considered tasks.
 544 This is interesting because it is in spite of the fact that reservoirs are smaller. On the other hand, for $b > 0$,
 545 we have a different behaviour, first in the memory task, performances are close even though $(K = 4,$
 546 $N = 2500)$ performs slightly better in the most difficult ($\tau = -14$) set-up. Second, in the prediction
 547 task, $(K = 4, N = 2500)$ and $(K = 8, N = 5000)$ give very similar performance, while the latter have
 548 reservoirs of twice the size. Surprisingly, even though $(K = 16, N = 10000)$ has the biggest network, its
 549 performance is way below the two others.

550 As a consequence, for the same given density value obtained with various combinations of K and N , we
 551 obtain distinct dynamics statistics and performance. We conclude that the density is not a control parameter
 552 for RBN reservoirs, and one must study the effect of K and N separately, as two independent control
 553 parameters.

554 Regarding the objective of the paper, these results suggest that K has a stronger influence on the
 555 performance than N , as increasing the size of the network does not necessarily guarantee higher
 556 performance, but reducing K consistently improves them.

7 OPTIMAL BALANCES FOR PERFORMANCE

| K | 1 | 2 | 3 | 4 | 5 | 8 | 16 |
|---------|--------|--------|--------|--------|--------|-------|-------|
| $b > 0$ | 0.024 | 0.024 | 0.052 | 0.029 | 0.077 | 0.149 | 0.179 |
| $b < 0$ | -0.099 | -0.069 | -0.057 | -0.029 | -0.049 | -0.52 | -0.99 |

Table 1. Table of the balance b_{opt} giving the best average performance at white-noise memory for $\delta = -18$ ($N = 10000$). The green highlight represents the optimal K value. Lower values of K typically give the lowest b_{opt} values, while increasing K tends to increase b_{opt} in absolute value.

| K | 1 | 2 | 3 | 4 | 5 | 8 | 16 |
|---------|-------|-------|-------|--------|-------|-------|-------|
| $b > 0$ | 0.95 | 0.19 | 0.068 | 0.024 | 0.098 | 0.15 | 0.19 |
| $b < 0$ | -0.24 | -0.20 | -0.12 | -0.047 | -0.42 | -0.82 | -0.95 |

Table 2. Table of the balance b_{opt} giving the best average performance at Mackey-Glass prediction for $\tau = 28$ ($N = 10000$). The green highlight represents the optimal K value, which typically gives the lowest b_{opt} values, while increasing K tends to increase b_{opt} in absolute value.

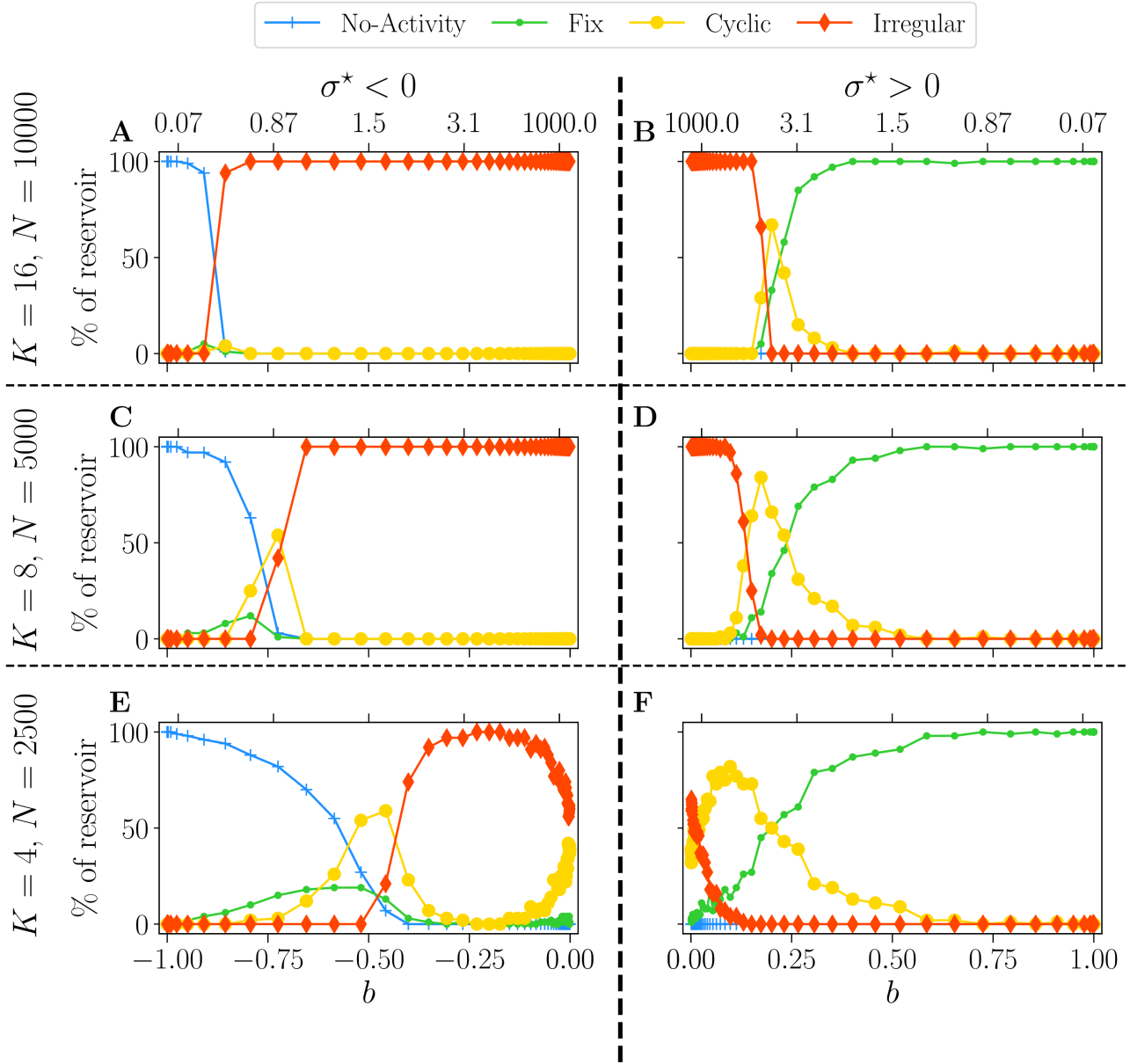


Figure 11. Attractor statistics of free-evolving RBN reservoirs, controlled by K and N with a constant ratio (rows), versus the balance b (x-axis). The lower x-axis represents the corresponding $|\sigma^*|$, for $b < 0$ (**A**, **C**, **E**), and $b > 0$ (**B**, **D**, **F**). Each steady activity signal is classified into one of the four categories of attractors: no-activity (+), fix (•), cyclic (●), irregular (◆). The statistics of attractors are computed over 100 reservoirs run once (y-axis). Results are shown for $K = 16, N = 10000$ (**A** and **B**), $K = 8, N = 5000$ (**C** and **D**), and $K = 4, N = 2500$ (**E** and **F**).

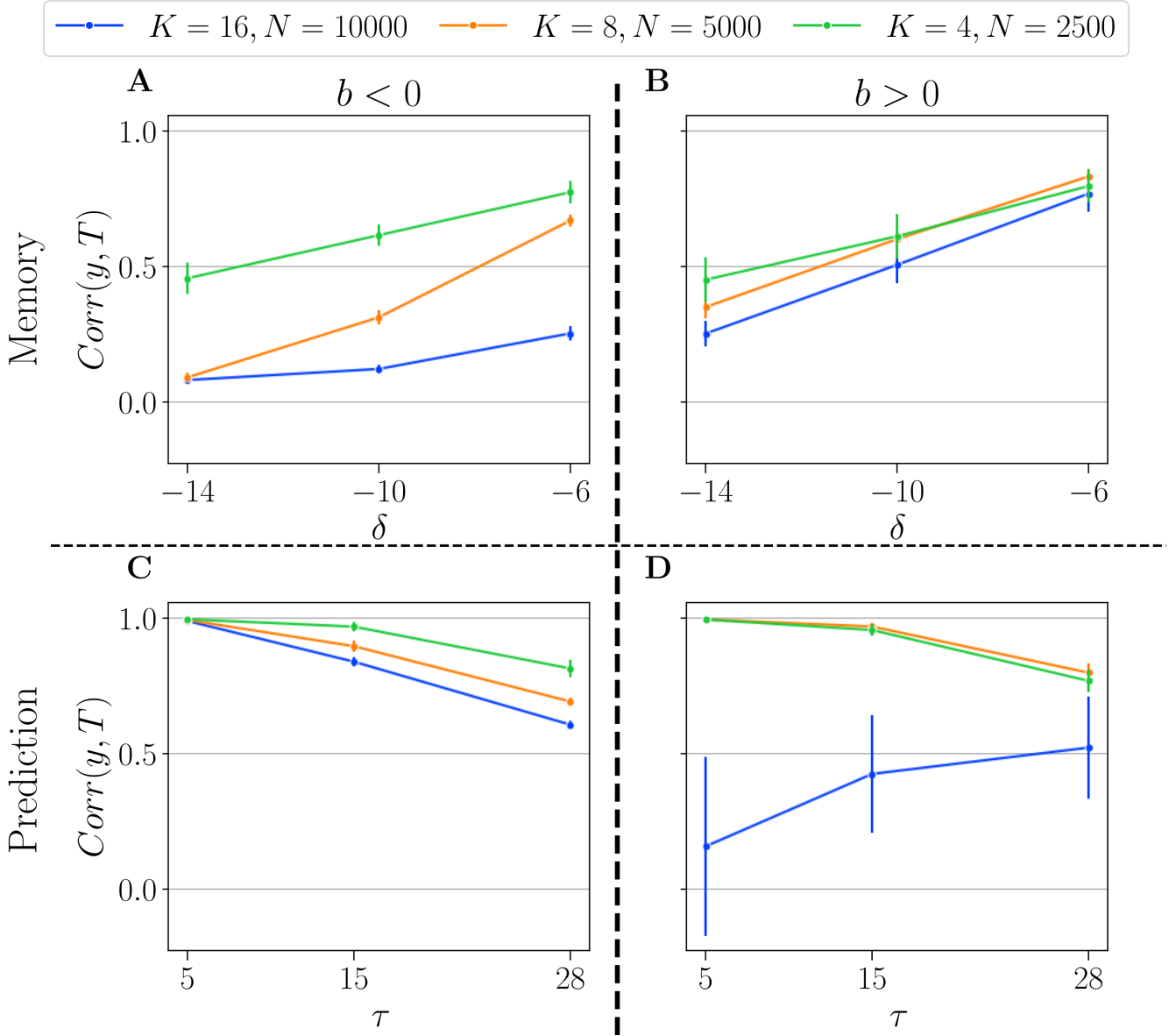


Figure 12. Summary of performance in the memory (**A** and **B**) and the prediction (**C** and **D**) tasks, for three couples of K and N resulting in the same density: $K = 4, N = 2500$; $K = 8, N = 5000$; and $K = 16, N = 10000$. Results are shown for both $b < 0$ (left panel), and $b > 0$ (right panel). For each value of (K, N) , we selected the b_{opt} giving the highest average performance, in the most difficult task ($\delta = -14$ for memory, and $\tau = 28$ for prediction). We plot the performance (higher is better) of reservoirs $\text{Corr}(y, T)$ (y-axis), plotted as a function of their respective task parameters (x-axis): δ (memory) and τ (prediction). The solid line represents the average over 20 reservoirs (generated with the same b_{opt} and (K, N) values. The error bars represent one standard deviation.